Compaction and possible differentiation of asteroid 21 Lutetia

Wladimir Neumann, Doris Breuer, Tilman Spohn
Deutsches Zentrum für Luft- und Raumfahrt

Introduction

In the present study[1], we model the thermo-chemical evolution of asteroid 21 Lutetia using new data obtained by the Rosetta flyby in July 2010. We investigate the dependence of the evolution on the accretion onset time and duration for both instantaneous accretion and continuous accretion scenarios, assuming late runaway material accumulation. The thermo-chemical evolution model considers accretion, compaction (sintering by hot pressing), melting and differentiation by porous flow. The evolution scenarios arising from assumptions on the present-day macroporosity φ_m are examined to derive implications on the compaction of an initially highly porous material, (partial) differentiation and the internal structure. The calculated final structures are compared with the observational data to derive bounds on the present-day macroporosity of Lutetia. Varying the macroporosity φ_m, we calculate the initial material properties such as intrinsic density, composition, and radiogenic heat source abundance, assuming an enstatitic origin of Lutetia's primordial material. We obtain a number of possible compaction and differentiation scenarios consistent with the properties of the present-day Lutetia.

Model

We use the model of a partially molten planetesimal from [2]. The heat conduction equation with a radiation boundary condition is modified to consider latent heat of melting and crystallization and also melt heat transport.

$$\rho c_p \left(1+x_{Fe}St_{Fe}+x_{Si}St_{Si}\right)\frac{\partial T}{\partial t}=\frac{1}{r^2}\frac{\partial}{\partial r}\left(kr^2\frac{\partial T}{\partial r}\right)+Q(r,t)+\left(\Delta v_{Fe}+\Delta v_{Si}\right)\frac{\partial T}{\partial r}$$

$$T(r,t_0)=T_n(t,d(t)) \qquad \left.\frac{\partial T}{\partial r}\right|_{r=0}=0 \qquad \left.\frac{\partial T}{\partial r}\right|_{r=R_p(t)}=\frac{e\sigma_{SB}}{k(R_p(t))}\left(T(t,R_p(t))^4-T_n^4\right)$$

The accretion is considered as radial growth by modifying the radius $R_p(t)$ via an asymptotical accretion law[3] $dR/dt \sim R^2$. In the initially porous state, the fit from [4] is used to account for the low thermal conductivity. Compaction of porous material obeys an Arrhenius-like porosity evolution law adopted from [5]. Thereby, the effective stress σ follows from the geometric model of [6].

$$\partial\log(1-\phi)/\partial t = 4.0\cdot10^{-5}\sigma(\phi)^{\frac{3}{2}}G^{-3}e^{-\frac{E}{RT}}$$

$$\sigma(\phi)=\sigma_0/\alpha\left(D^{2/3}\beta^{2/3}h^2-1\right)$$

ϕ	porosity
G	grain size
E	activation energy
R	gas constant
D	relative density
α, β, h	geometric parameters

Melt segregating from the solid matrix transports the energy of the hot material, increasingly with progressing melting. This process is treated as a flow in porous media, where the melt velocity is computed from the Darcy flow equation:

$$\Delta v = K_\psi\left(\rho_l-\rho_s\right)g/\psi\eta$$

$K_\psi=b^2\varphi^n/\pi\eta$	permeability	b	grain size
η	melt viscosity	ψ	melt volume fraction
ρ_s	martix density	ρ_l	melt density
		n, T	geometric constants

In a partially molten system small particles dissolve and redeposit on the surfaces of larger crystals (Ostwald ripening):

$$b^3=b_0^3+8v^2\gamma cdt/9RT$$

v	molar volume	γ	surface free energy
c	solute concentration	d	diffusion coefficient
R	gas constant	T	temperature

Initially homogeneous distribution of the heat producing nuclei changes due to the chemical differentiation, as it depends on the fractions of iron and silicates. Furthermore ^{26}Al is enriched in the silicate melt:

$$c_{Al}^{tot}=\chi_{Si}c_{Al}^{l}+(1-\chi_{Si})c_{Al}^{s} \qquad c_{Al}^{l}=\frac{c_{Al}^{tot}}{P+\chi_{Si}(1-P)} \qquad c_{Al}^{s}=\frac{c_{Al}^{tot}P}{P+\chi_{Si}(1-P)}$$

		c	concentration,
P			partition coeffitient,
l , s			liquid, solid,
χ_{Si}			silicate melt fraction

Theory

Table 1. Mass and volume fractions of the iron and silicate phases and average thermal conductivity of the mixed phases (assuming zero porosity) as a function of the macroporosity.

Macro-porosity [%]	Intrinsic density [kg m^{-3}]	Initial bulk density [kg m^{-3}]	Phase	Mass fraction [%]	Volume fraction [%]	Thermal conductivity [W m^{-1}K^{-1}]	Fe/Al mass fraction [%]	Abundance of Fe / Al [kg^{-1}]
0	3400	2040	Iron	19.19	9.07	4.34	17.40	$1.75\cdot10^{24}$
			Silicates	80.81	90.93		0.74	$1.72\cdot10^{23}$
4	3542	2125	Iron	25.31	12.45	4.56	22.96	$2.30\cdot10^{24}$
			Silicates	74.69	87.55		0.69	$1.59\cdot10^{23}$
5	3579	2147	Iron	26.84	13.35	4.62	24.35	$2.44\cdot10^{24}$
			Silicates	73.16	86.65		0.67	$1.56\cdot10^{23}$
6	3617	2170	Iron	28.38	14.26	4.69	25.74	$2.58\cdot10^{24}$
			Silicates	71.62	85.74		0.66	$1.53\cdot10^{23}$
8	3696	2217	Iron	31.44	16.14	4.82	28.52	$2.86\cdot10^{24}$
			Silicates	68.56	83.86		0.63	$1.46\cdot10^{23}$
13	3908	2345	Iron	39.10	21.23	5.19	35.47	$3.56\cdot10^{24}$
			Silicates	60.90	78.77		0.56	$1.30\cdot10^{23}$
25	4533	2720	Iron	57.48	36.21	6.47	52.14	$5.23\cdot10^{24}$
			Silicates	42.52	63.79		0.39	$0.91\cdot10^{23}$

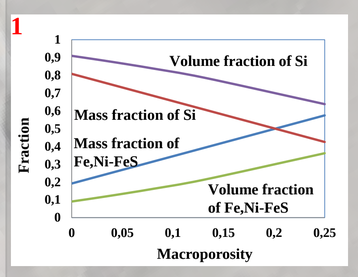

Fig. 1. Initial mass (red line for silicates and blue line for iron) and volume fractions (purple line for silicates and green line for iron) of the phases

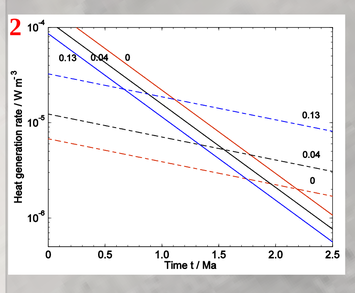

Fig. 2: Heat generation rate by ^{26}Al (solid lines) and ^{60}Fe (dashed lines) per 1 m^3 of the undifferentiated sintered material for φ_m=0 (red lines), φ_m=0.04 (black lines) and φ_m=0.13 (blue lines), assuming ρ_b=3400 kg m^{-3}. With increasing macroporosity, the crossover time, at which the heating rate by ^{60}Fe dominates over the heating rate by ^{26}Al, moves to earlier times.

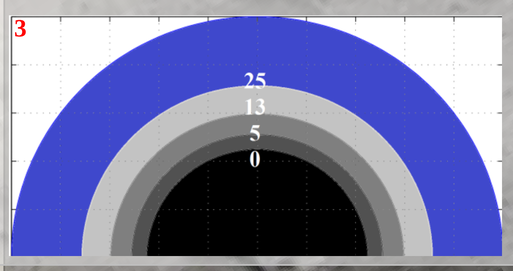

Fig. 3. Maximum relative core size of a completely compacted and differentiated body for different macroporosities assuming ρ_b=3400 kg m^{-3}.

Results

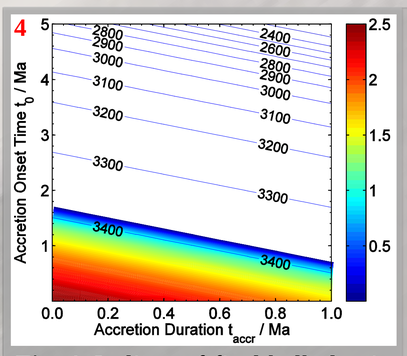

Fig. 4. Isolines of final bulk density in kg m^{-3} are given along with the core radius. The core radius is colour coded according to the scale on the right-hand side of the figure in units of tens of km. The models have ρ_i=3579. The successful model has a bulk density of 3400 kg m^{-3} and a macroporosity of φ_m=0.05.

Fig. 5. The final bulk density (solid blue lines) and core size (in km; dot-dashed brown lines) as functions of the intrinsic density (macroporosity, in %) and the formation time t_0 relative to CAIs formation: a) ρ_b=3100 kg m^{-3}, b) ρ_b=3400 kg m^{-3}, c) ρ_b=3700 kg m^{-3}. The green dot-dashed lines show the maximum temperature $T_{S,Fe}$=1213 K. Note that the isolines for $T_{S,Si}$=1425 K almost coincides with the isolines for the core size of 5000 m and are not plotted here for clarity. The present-day bulk density is reached for the macroporosities between 4.1% and 4.4%, 4% and 6%, and 3.7% and 6.2% for the present-day bulk density of 3100, 3400, and 3700 kg m^{-1}.

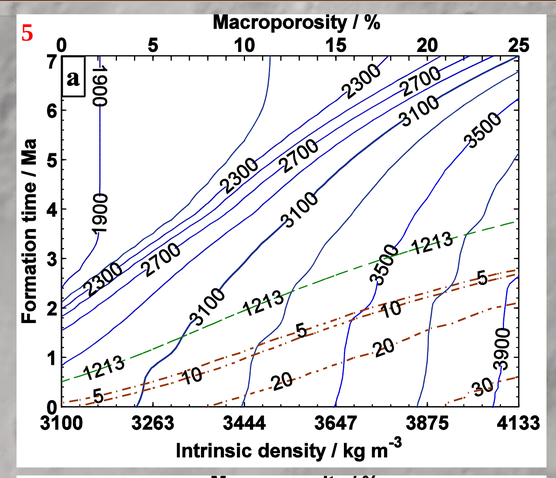

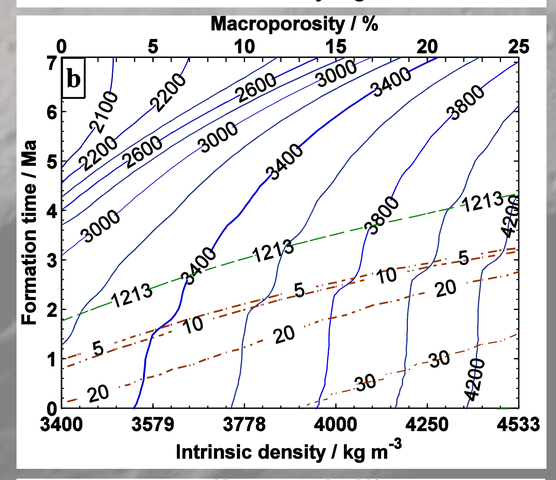

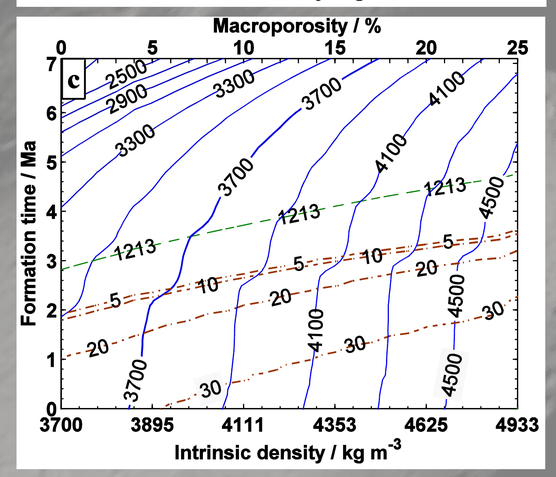

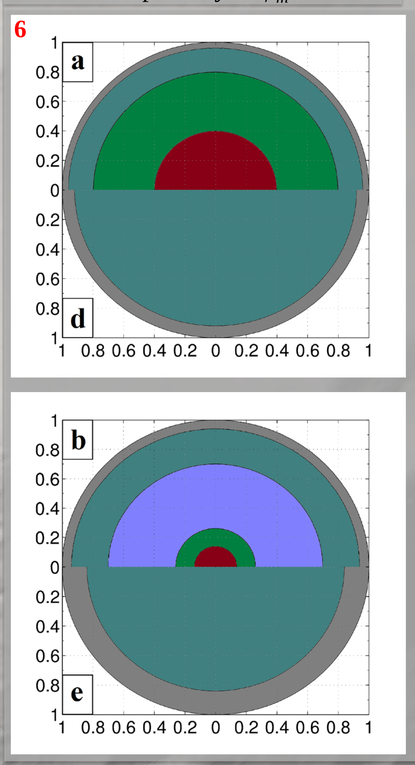

Fig. 6. Final structure of the bodies for ρ_b=3400 kg m^{-3}. Panels **a-f** correspond to the parameters ρ_i=3542, 3579, 3617, 3696, 3908 and 4533 kg m^{-3} (φ_m=0.04, 0.05, 0.06, 0.08, 0.13, 0.25), respectively.

- iron core
- silicate mantle
- undifferentiated partially molten region
- unmelted sintered region
- unsintered layer

Conclusions

- a variety of possible structures with the present-day bulk density is obtained
- formation times range from 0 to ≈8 Ma relative to the CAI´s
- $\varphi_m \geq 0.04$ is necessary to obtain ρ_b=3400 kg m^{-3}
- internal structures range from partially differentiated to highly porous with varying degree of thermal metamorphism without melting
- differentiated interior is possible for $0.04 \leq \varphi_m < 0.06$
- in a such case the core radius is less than 25 km
- this argues against the estimates of Weiss et al. 2012 who suggest that differentiated interior is only indicated for $\varphi_m > 0.13$
- no melt eruptions at the surface are observed, which corresponds to the lack of basaltic crust on Lutetia
- the results are robust relative to the variation within the interval ρ_b=3400±300 kg m^{-3}

Acknowledgement

This research has been supported by the DFG Priority programme 1385 "The First 10 Million Years of the Solar System - a Planetary Materials Approach" and by the Helmholtz Association through the research alliance "Planetary Evolution and Life".

References

[1] Neumann, W. et al. 2013. The thermo-chemical evolution of asteroid 21 Lutetia. Icarus 224, 126-143.
[2] Neumann, W. et al., Differentiation and core formation in accreting planetesimals, Astronomy and Astrophysics 543, A141, 2012.
[3] Kortenkamp, S. J. et al. 2000. Formation of planetary embryos. In: Origin of the Earth and Moon. The University of Arizona Press., Tucson, Arizona.
[4] Krause, M. et al. 2011. Modeling the early thermal evolution of meteorite parent bodies based on the thermal conductivity measurements of highly porous aggregates, Abstract, LPSC 2011, #2696, 2011.
[5] Schwenn, M. B., Goetze, C. 1978. Creep of olivine during hot-pressing. Tectonophysics 48, 41-46.
[6] Rao, A. S., Chaklader, A. C. D. 1972. Plastic flow during hot-pressing. Journal of the American ceramic society 55, 596-601.